Five Coplanar Anion Binding Sites on One Face of Phospholipase A_2: Relationship to Interface Binding[†,‡]

Ying H. Pan, Todd M. Epstein, Mahendra K. Jain, and Brian J. Bahnson*

Department of Chemistry and Biochemistry, University of Delaware, Newark, Delaware 19716

Received November 1, 2000; Revised Manuscript Received December 5, 2000

ABSTRACT: We report the structures of the crystallographic dimer of porcine pancreatic IB phospholipase A_2 (PLA2) with either five sulfate or phosphate anions bound. In each structure, one molecule of a tetrahedral mimic MJ33 [1-hexadecyl-3-(trifluoroethyl)-*sn*-glycero-2-phosphomethanol] and the five anions are shared between the two subunits of the dimer. The *sn*-2-phosphate of MJ33 is bound in the active site of one subunit (A), and the alkyl chain extends into the active site slot of the second subunit (B) across the subunit−subunit interface. The two subunits are packed together with a large hydrophobic and desolvated surface buried between them along with the five anions that define a plane. The anions bind by direct contact with two cationic residues (R6 and K10) per subunit and through closer-range H-bonding interactions with other polarizable ligands. These features of the "dimer" suggest that the binding of PLA2 to the anionic groups at the anionic interface may be dominated by coordination through H-bonding with only a partial charge compensation needed. Remarkably, the plane defined by the contact surface is similar to the i-face of the enzyme [Ramirez, F., and Jain, M. K. (1991) *Proteins*: *Struct*., *Funct*., *Genet*. *9*, 229−239], which has been proposed to make contact with the substrate interface for the interfacial catalytic turnover. Additionally, these structures not only offer a view of the active PLA2 complexed to an anionic interface but also provide insight into the environment of the tetrahedral intermediate in the rate-limiting chemical step of the turnover cycle. Taken together, our results offer an atomic-resolution structural view of the i-face interactions of the active form of PLA2 associated to an anionic interface.

Evaluation of the structural basis for the activation of interfacial enzymes is arguably one of the major unresolved areas in enzymology. The 14 kDa family of secreted phospholipase A_2 enzymes (PLA2,[1] EC 3.1.1.4), which catalyze the hydrolysis of the *sn*-2-acyl substituent of glycerophospholipids, has become the prototype for interfacial enzymology (*1*, *2*). These water-soluble enzymes associate to an organized interface as a functionally active monomer to access their substrate, and processively carry out the catalytic turnover (*1*−*5*) as depicted in Scheme 1. PLA2 must make critical and specific interactions along its interface-binding surface (i-face) to reach its fully activated form on an interface (*6*). Once associated to the membrane surface along the i-face, E* binds a substrate molecule, S*, from the aggregated substrate interface. The resulting E*S complex then undergoes an additional change on an anionic interface to give an activated Michaelis complex $(E^*S)^{\#}$ (*3*), which undergoes esterolysis in the chemical step to form products.

Scheme 1

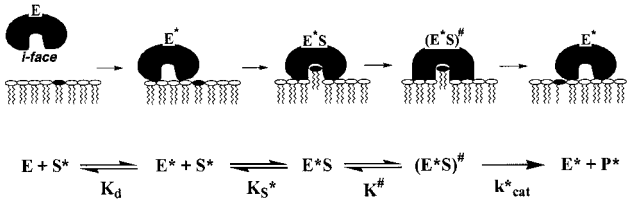

Specifically, pancreatic PLA2 requires anionic charges at the interface to attain optimal activity (*3*, *5*, *7*, *8*). Here, a significantly higher rate of reaction was observed for PLA2 binding to an anionic interface and the consequent allosteric k^*_{cat} activation, which gives rise to the $(E^*S)^{\#}$ activated complex in Scheme 1. The physiological significance of this activation is consistent with the environment of the natural substrate for the pancreatic PLA2 that is codispersed with anionic bile salts. Ultimately, the structural features of interest for interfacial enzymology are the i-face and the catalytic active site, which may or may not be functionally coupled.

A high-resolution structural perspective of the kinetically significant interactions and potential conformational changes of the E* forms has been lacking due to the experimental difficulty of determining macromolecular structures of proteins associated with an interface (*1*, *2*, *9*). However, low-

[†] The research was supported by NIH Grant GM-29703 (M.K.J.), NIH Training Grant T32 GM-08550 (T.M.E.), and a grant from the University of Delaware Research Foundation (B.J.B.).

[‡] Coordinates for the structure of phospholipase A_2 complexed with phosphate anions (1FXF) or sulfate anions (1FX9) have been deposited in the Protein Data Bank.

* To whom correspondence should be addressed. E-mail: bahnson@udel.edu. Phone: (302) 831-0786. Fax: (302) 831-6335.

[1] Abbreviations: *B*-factor, temperature factor; i-face, interface binding surface of an enzyme; MJ33, 1-hexadecyl-3-(trifluoroethyl)-*sn*-glycero-2-phosphomethanol; MPD, 2-methyl-2,4-pentanediol; PDB, Protein Data Bank; PLA2, phospholipase A_2; P-structure, PLA2 dimer with bound phosphate anions; QM/MM, quantum-mechanical/molecular-mechanical; R_{free}, free *R*-factor; $R_{working}$, working *R*-factor; rmsd, root-mean-square deviation; S-structure, PLA2 dimer with bound sulfate anions; 69-loop, residues 59−75 of PLA2.

10.1021/bi002514g CCC: $20.00
Published on Web 12/29/2000

resolution information from spectroscopic methods (*3*, *6*, *7*, *9*−*11*) has been useful for identifying the specific interactions between the interface and domains of PLA2. The majority of previously reported PLA2 crystal structures (*3*, *9*, *12*−*17*) were determined from protein crystals grown using 2-methyl-2,4-pentanediol (MPD) as a precipitant with few or no salts added. Consequently, an atomic-resolution structural perspective that reveals the location of the anion binding sites on the i-face is lacking.

We set out to identify anionic binding sites of PLA2 by searching for new crystallization conditions that included anions that could mimic the phosphatidyl group of an anionic lipid bilayer. We have determined the crystal structures of a dimeric form of the PLA2 enzyme with bound sulfate (S-structure) or phosphate anions (P-structure). Surprisingly, these anionic binding sites are coplanar and interact with the same face of PLA2 in both subunits of the dimer. Additionally, the structures reported are unusual in that two subunits of PLA2 have come together in each crystallographic asymmetric unit with a single molecule of the competitive inhibitor shared between their two facing active sites. The plane defined by these anions and the subunit−subunit contact surface is remarkably similar to the proposed i-face surface of the enzyme. Therefore, these structures offer a structural view of the enzyme that models a single catalytic subunit of PLA2 on an interface in its active form.

EXPERIMENTAL PROCEDURES

Crystallization and X-ray Data Collection. Porcine pancreatic PLA2 and the competitive inhibitor [1-hexadecyl-3-(trifluoroethyl)-*sn*-glycero-2-phosphomethanol] (MJ33) were obtained as described previously (*18*). Crystals of the PLA2−MJ33 complex were grown at 25 °C, from 2.5 μL hanging drops containing 15 mg/mL (1 mM) PLA2, 3 mM MJ33, 10 mM $CaCl_2$, 25% PEG 3500, 0.1 M sodium acetate, and 0.2 M $(NH_4)_2SO_4$ for the S-structure or NaH_2PO_4 for the P-structure with the final pH adjusted to 4.6. Almost cubic crystals appeared in 3 days and grew to dimensions of 0.5 mm × 0.5 mm × 0.5 mm after 7 days.

X-ray diffraction data sets were collected from a single crystal on a Rigaku-RU300 rotating anode generator with a RAXIS IV image plate area detector. The crystals were pre-equilibrated in a cryoprotecting and stabilizing solution made of the crystallization condition with the addition of xylitol as the cryoprotectant at a concentration 25% of saturating and then flash-frozen in the −180 °C nitrogen cryostream. The programs DENZO and SCALEPAK (*19*) were used for data processing and scaling. The sulfate- or phosphate-bound PLA2−MJ33 crystals were indexed and processed in the trigonal space group, consistent with either space group $P3_1$ or $P3_2$ on the basis of scaling statistics.

Molecular Replacement. The crystal structure of the S-structure form of the PLA2−MJ33 complex was determined by molecular replacement using the program AMORE from the CCP4 package (*20*). The model used for molecular replacement was the porcine PLA2 structure [Protein Data Bank (PDB) entry 4P2P] previously reported (*16*) minus water molecules. In both space groups $P3_1$ and $P3_2$, two rotational solutions were found. However, a reasonable translation solution was found only in the $P3_1$ space group. The final molecular replacement solution included two subunits of PLA2 in the asymmetric unit with an *R*-value of 46.6% and a correlation factor of 40.8%.

Crystallographic Refinement. Initial refinement of the S-structure crystal form of the PLA2−MJ33 complex was carried out using the program X-PLOR (*21*) with standard refinement procedures, such as rigid body, simulated annealing, positional, and individual temperature factor (*B*-factor) refinement. The model was improved iteratively through model adjustment using the graphics programs CHAIN (*22*) and O (*23*) and further rounds of X-PLOR refinement. The refinement of the S-structure converged to a free *R*-factor (R_{free}) of 0.298 and a working *R*-factor ($R_{working}$) of 0.230. Regions involving residues Lys-62, Phe-63, Leu-64, Val-65, and Asp-66 were found to have a conformation significantly different from that of the original molecular replacement search model and were manually rebuilt. The P-structure of the PLA2−MJ33 complex, which is isomorphous to the S-structure, was refined by directly starting from a model of the partially refined S-structure. Similarly, in the P-structure, X-PLOR refinement at 1.85 Å converged to yield an R_{free} of 0.302 and an $R_{working}$ of 0.219.

Hemihedral Twinning. Although the refinement statistics were suggestive of a good model for each structure at this point, there were indications of problems with the model. Most notably, the electron density around MJ33 suggested disorder of the inhibitor. This was particularly troubling as it placed ambiguity on the position of the *sn*-2 carbon and the *sn*-3 trifluoromethyl group of MJ33. The possibility that this disorder is the result of crystallographic hemihedral twinning (*24*) was investigated. A form of hemihedral twinning, called merohedral twinning, was detected from this analysis. Merohedral twinning can occur when crystals have distinct domains that are oriented in alternate conformations, and the resulting twinned lattices superimpose perfectly. The twin operation and twin fraction were identified and quantified using previously reported methods (*25*), where the S- and P-structure crystal forms both exhibited a partial twinning fraction of >0.4.

Crystallographic refinement, which included twin corrections, was performed using the programs CNS (*26*) and SHELXL-97 (*27*). Initially, refinement using a twin correction was focused on the P-structure using the program CNS. One round of positional and individual *B*-factor refinement using a twinning fraction of 0.43 lowered the values of R_{free} and $R_{working}$ to 0.239 and 0.179, respectively. However, the electron density maps were still not adequately interpretable in the inhibitor region to resolve the ambiguities mentioned above. The model was then refined using the program SHELXL-97. Without the inhibitor in the model, 10 cycles of conjugated gradient least-squares refinement with a standard twinning refinement gave R_{free} and $R_{working}$ values of 0.261 and 0.188, respectively. The resulting $2F_o - F_c$ electron density maps were good enough to correctly place the *sn*-2-glycerol carbon and the rest of the MJ33 inhibitor into a well-defined orientation, and refinement was completed.

RESULTS

The initial goal of this study was to define the anionic binding sites of PLA2. This goal was achieved following the successful crystallization with phosphate or sulfate anions

Table 1: Data Collection and Refinement of the S- and P-Structures

	S-structure	P-structure
anions bound	five sulfates	five phosphates
space group	$P3_1$	$P3_1$
cell parameters		
$a = b$ (Å)	64.99	65.04
c (Å)	62.77	62.75
no. of subunits per asymmetric unit	2	2
X-ray data		
total no. of reflections	122013	215840
no. of unique reflections	19393	25141
resolution limit (Å)	2.0	1.85
completeness (%)	96.5	99.1
R_{merge}[a]	0.068	0.059
refinement		
resolution range (Å)	8−2.0	8−1.85
$R_{working}$[b]	0.171	0.161
R_{free}[b]	0.222	0.267
rmsd[c] (observed)		
bond lengths (Å)	0.006	0.007
angle distances (Å)	0.023	0.027
total no. of non-hydrogen atoms	2303	2569
total no. of water molecules	188	280

[a] $R_{merge} = \Sigma|I_o - I_a|/\Sigma(I_a)$, where I_o is the observed intensity and I_a is the average intensity, the sums being taken over all symmetry-related reflections. [b] R-factor $= \Sigma|F_o - F_c|/\Sigma(F_o)$, where F_o is the observed amplitude and F_c is the calculated amplitude. R_{free} is the equivalent of $R_{working}$, except it is calculated for a randomly chosen set of reflections that were omitted (10%) from the refinement process (*40*). [c] Root-mean-square deviation.

bound to the enzyme dimer. The statistics of the data collection and refinement of the sulfate- and phosphate-bound forms of PLA2 complexed with MJ33 are summarized in Table 1. The S- and P-structures are isomorphous, as shown by an alignment over all the C_α atoms that exhibited a root-mean-square deviation (rmsd) of 0.304 Å, indicating the protein backbones are virtually identical. These structures are likewise quite similar to previously reported pancreatic PLA2 structures. For example, an alignment over all the C_α atoms between the P-structure and a monomeric bovine PLA2 structure (PDB entry 1FDK) with MJ33 bound (*12*) has an rmsd of 0.943 Å.

Anion Binding Sites. During model refinement using difference electron density maps, clear electron densities appeared that were interpreted as well-ordered sulfate or phosphate anions. The final S- and P-structures are isomorphous, each with five sulfate or phosphate anion binding sites per crystallographic dimer. Figure 1a shows the PLA2 dimer from the P-structure with the positions of bound phosphate anions displayed. The anion coordinating ligands from the protein side chains, backbone, and bound water are listed in Table 2 for both the S- and P-structures. The striking result is that all five of these anionic binding sites are nearly coplanar, and furthermore lie on one surface of a single functional subunit of PLA2. Also noteworthy is the fact that the contact face and protein ligands to bound anions are virtually the same for both subunits A and B.

The PLA2 Dimer Shares One Inhibitor. Each subunit of the S- and P-structure dimers has a calcium bound in its calcium binding loop (Figure 1a). However, the two subunits share a single molecule of the competitive inhibitor MJ33. The *sn*-2 phosphate of MJ33 is coordinated to the calcium in subunit A. The hexadecyl tail extends out of subunit A into the active site of the neighboring subunit B of the contact dimer pair. The alkyl tail exhibited two alternate conformations with occupancies for the major and minor conformations of 0.7 and 0.3, respectively. The final refined S- and P-structures exhibited clear electron density for the entire MJ33 molecule as shown in Figure 1b with a representative electron density map for the P-structure.

The 69-Loop Is Ordered at the Subunit−Subunit Contact Surface. In addition to PLA2 interactions with the bound anions, there is a close-contact surface defined between the two subunits of the contact dimer that is shielded from the solvent channels of the crystal. The residues that contact the neighboring subunit across the subunit interface are displayed in Figure 1c for interactions in the P-structure. The 69-loop (residues 59−75), named for the mechanistically critical residue Tyr-69, is often disordered in other PLA2 crystal structures. In both subunits of the P- and S-structures, this loop is ordered with all the side chains built in. The side chains displayed in the subunit−subunit contact surface in Figure 1c include Val-65, Asp-66, Tyr-69, and Thr-70 from the 69-loop.

PLA2 Active Site and Tetrahedral Mimic. The P-structure interactions that MJ33 makes with active site residues, including the calcium and active site waters w6 and w12, are shown in Figure 1b. The *sn*-2 phosphate of MJ33 is coordinated to the calcium of subunit A. The P-structure has a seven-coordinate calcium with w12 in the axial coordination site (Figure 1b). Interestingly, a second water (w6), which was observed in both P- and S-structures, bridges His-48 and the *pro-S* oxygen from the *sn*-2 phosphate of MJ33. Additionally, Tyr-69, which is a critical residue from the 69-loop, is also H-bonding with the same *pro-S* oxygen of MJ33, as shown in Figure 1b.

DISCUSSION

The S- and P-structures of porcine PLA2 are generally consistent with the reported structures of 14 kDa secreted PLA2 (*3*, *9*, *12*−*17*). The differences are, however, significant in obtaining insights into the binding of the i-face to an interface and for the events of the chemical step at the active site. Interfacial catalysis (Scheme 1) is defined by the need of an enzyme to associate with a substrate interface to processively access the substrate for the catalytic cycle. Therefore, the challenge is to develop an experimentally tractable method for obtaining mechanistically interesting structures. We believe that our strategy to induce the formation of an anion-bridged crystallographic dimer may offer a general strategy for obtaining structural clues for the changes that occur to the enzyme in assuming an activated form on an anionic interface. Key insights from this work are developed below.

The Anion Binding Sites. Structures of PLA2 with either phosphate or sulfate anions bound reveal the potential interactions of the enzyme that account for its anionic interface charge preference. The use of sulfate or phosphate anions during crystal growth turned out to be critical for the formation of the dimer form of PLA2, to ligate residues and bridge the adjoining subunits along the i-face. Note that the protein ligands that are in direct contact with each bound anion are symmetrically provided by two subunits from opposite sides of the i-face. Also, cationic residues only partially account for the expected charge neutralization required upon anion binding. Results in Table 2 show that

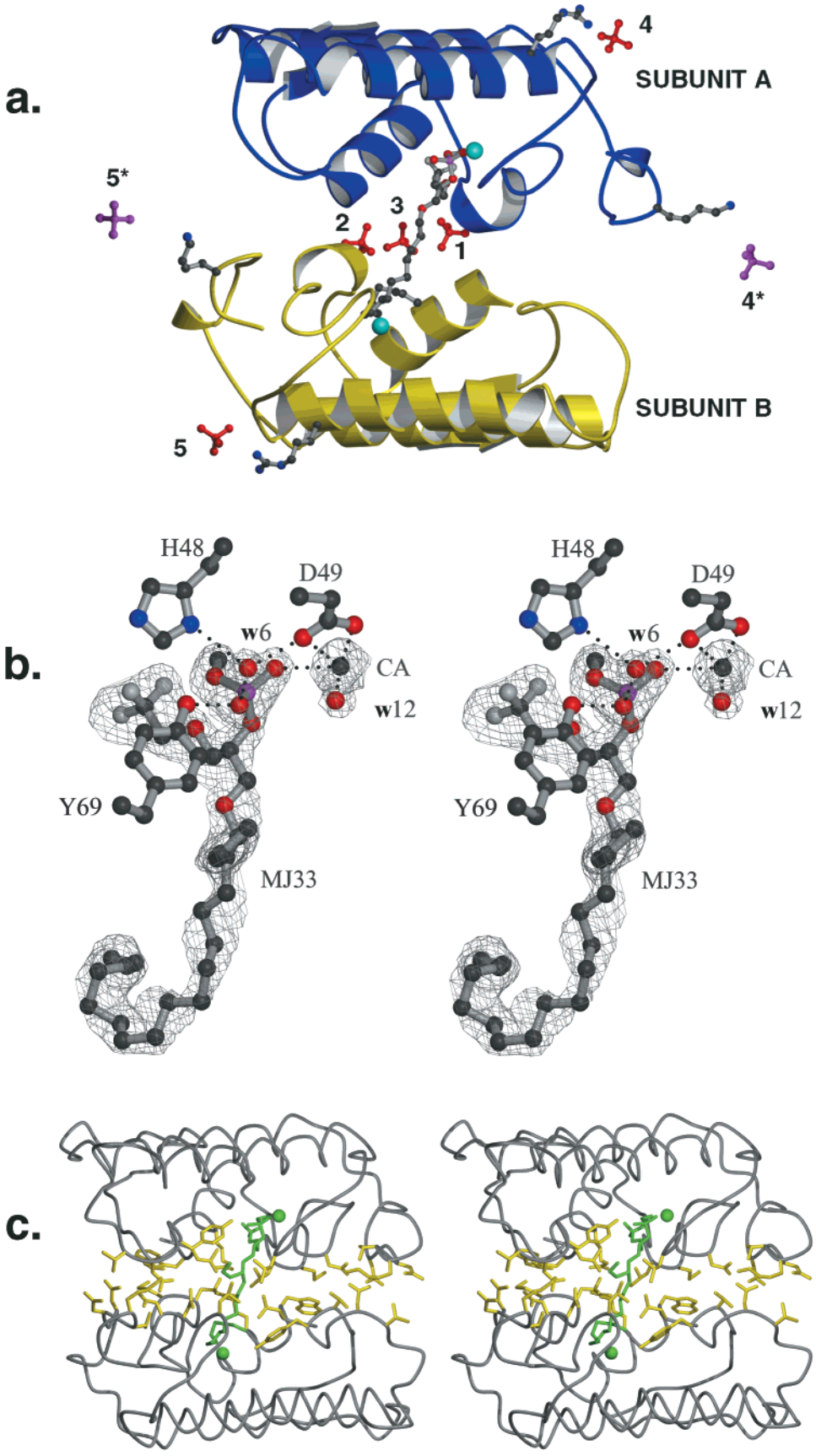

FIGURE 1: Crystal structure of PLA2 with phosphate anions bound. (a) PLA2 crystallographic dimer with MJ33 shared between two subunits that have five coplanar bridging phosphate anions. The calcium of subunit A is coordinated to the *sn*-2 phosphate of MJ33. The alkyl tail of the inhibitor crosses the subunit−subunit interface and occupies the active site of the partner subunit, B. Phosphate anions 1−5 (numbering consistent with Table 2) are in red, and anions 4* and 5* are in purple. Positions 4* and 5* are crystallographically identical to anion sites 4 and 5, respectively (Table 2). The interaction with position 4* or 5* is mediated by a bridging water molecule, in each case,

Table 2: Coordination of Phosphate and Sulfate Anions in the P- and S-Structures of Porcine Pancreatic PLA2[a]

anions	residue/atom type	subunit	distance (Å)	anions	residue/atom type	subunit	distance (Å)
PO_4 (1)				SO_4 (1)			
O1	R6, NH2	B	3.10	O1	R6, NH2	B	3.02
	w125		2.34	O2	R6, Nϵ	A	2.84
O2	R6, Nϵ	A	2.97		L19, N	A	2.89
	L19, N	A	2.85	O3	R6, NH1	A	2.91
O3	R6, NH1	A	3.22		w23		2.62
	w197		2.54	O4	M20, N	A	3.25
O4	L19, N	A	3.41	SO_4 (2)			
PO_4 (2)				O1	R6, NH2	A	3.28
O1	R6, NH2	A	2.70		w63		2.63
	w180		2.91	O2	R6, Nϵ	B	2.59
O2	R6, Nϵ	B	2.62		L19, N	B	2.92
	L19, N	B	2.59	O3	R6, NH1	B	2.50
O3	R6, NH1	B	2.49		w84		3.19
	w235		3.24	O4	M20, N	B	2.74
O4	L19, N	B	3.34	SO_4 (3)			
	M20, N	B	3.20	O1	w38		2.78
PO_4 (3)					w197		3.00
O2	R6, NH2	B	3.01	O2	w84		3.20
	w197		2.76	O3	R6, NH2	B	3.00
	K10, N_Z	B	2.50		w23		2.67
O3	R6, NH1	B	2.95	O4	R6, NH1	A	3.12
	w235		2.94	SO_4 (4)			
O4	R6, NH1	A	2.77	O3	E40, N	A	2.52
	K10, N_Z	A	3.24		w2		2.34
PO_4 (4)				O4	N112, $O_{\delta 1}$	A	3.43
O1	w170		2.37	SO_4 (5)			
O2	w205		3.07	O1	N112, $O_{\delta 1}$	B	2.95
	w206		2.59		w100		3.10
	w244		2.84		w179		2.44
	w250		2.69	O2	E40, N	B	2.99
O3	E40, N	A	2.74		w185		2.63
	w205		2.30	O3	w179		3.04
O4	N112, $O_{\delta 1}$	A	2.99	O4	w109		2.68
	w23		2.99		w163		2.38
	w244		3.09		w165		2.94
PO_4 (5)							
O1	N112, $O_{\delta 1}$	B	3.10				
O2	w63		2.88				
O4	N112, $O_{\delta 1}$	B	3.31				
	w11		2.29				

[a] Distances are listed for all protein side chains and ordered water molecules showing H-bonding interactions <3.5 Å long with the five phosphate anions and five sulfate anions of the P- and S-structures.

each bound anion has a partial charge compensation from an average of seven H-bonding and polarizable ligands, including water molecules. Comparable behavior for the binding of anions to other proteins has been reported from the examination of 52 anion binding sites in 34 proteins (*28*). Among these, only one structure, the photoreaction center protein (PDB entry 1PRC), had more than one or two anion binding sites (*29*). Quite remarkably, six of its seven bound sulfates lie in a plane, which defines where the membrane−aqueous interface is for this transmembrane protein. These coplanar anion binding sites likely orient the photoreaction center protein into an optimal geometry, analogous to what we think occurs when PLA2 binds anionic charges fixed on an interface. The other noteworthy observation from previously reported sulfate and phosphate protein binding sites (*28*) is that the negative charge on the bound anions is typically only partly neutralized, leaving other noncationic ligands to provide H-bonding groups on a hydrophobic face.

The i-Face. The five bound anions of the S- and P-structures define a plane. This is analogous to what PLA2 would "see" on an anionic interface where the phosphate moieties would lie roughly in a plane unless disturbed by the binding of the enzyme. The membrane-associated PLA2 enzyme would sit on this plane of anionic phosphatidyl

FIGURE 1: (Continued) to residue Lys-122 near the C-terminus from each subunit. Phosphate anions 1−3, 4*, and 5* are nearly coplanar, analogous to the charged surface presented to an interfacial enzyme by an anionic interface. (b) Representative electron density map ($2F_o - F_c$ coefficients) from the P-structure (stereoview). The MJ33 inhibitor is shown coordinated to the catalytic calcium ion. Also shown are essential residues His-48, Asp-49, and Tyr-69 and the active site calcium and its axial bound water (w12). The water that represents the assisting water of the mechanism is labeled w6. (c) The interface contact surface of the P-structure (stereoview). The inhibitor MJ33 and two calcium ions are in green. The side chains of each subunit that are within 5 Å of the subunit across the interface are in yellow. The 19 residues included (nonpolar, L2, W3, L19, M20, L31, V65, and L118; polar, N23, N24, D66, N67, Y69, T70, S72, N117, D119, and T120; and cationic, R6 and K121) have been identified as interfacial residues by a buried surface accessibility calculation (*41*). Bound water molecules are included in this calculation. In the P-structure, the total surface area for the complex of both molecules is 12 860 Å^2, of which 1470 Å^2 is buried at the interface. This figure was made using the programs MOLSCRIPT (*42*), POVSCRIPT (E. Peisach and D. Peisach, Brandeis University, Waltham, MA), and POVRAY (http://www.povray.org).

groups. Although the anionic charge at the interface is necessary for the binding of the enzyme, it does not necessarily follow that cationic residues on the protein directly participate in the close contact. Further insight into the significance of charge compensation comes from the inclusion of all the interactions of the bound anions, which are inaccessible to the bulk solvent. Specifically, backbone amides, bound water molecules, and more remote ionic interactions make up the majority of interactions.

The van der Waals surface footprint of the P-structure contact surface is shown in Figure 2a. The anionic binding sites are clustered in three functionally significant regions: the C-terminus, the N-terminus, and the 69-loop. The orientation and features of this footprint are strikingly similar to the proposed i-face contact surface (*6*). This model has been useful to account for virtually all the observations related to the i-face binding and activation events. Now one can develop a more detailed understanding at the level of specific interactions that characterize the close contact of E* with the interface. For example, the residues of subunit A that contact subunit B are also predicted to contact the interface of an aggregate substrate. The alkyl tail of MJ33, seen projecting out of the footprint (Figure 2a), is in an orientation that would allow it to remain in close apposition with, if not partially imbedded in, a bilayer (Scheme 1). Also note that many of the structural features of the i-face of PLA2 are localized such that their perturbation may account for the cross-talk noted in the functional and spectroscopic behavior related to the E*S to $(E^*S)^{\#}$ allosteric change (*3*). On the basis of this view, the binding of anions by residues that lie along the edge of the i-face brings the pancreatic PLA2 to its optimal catalytic geometry.

The net energetic drive for PLA2 binding to an anionic interface is about 15 kcal/mol of PLA2 (*30*). The hydrophobic effects and close-range H-bonding interactions along the 1470 Å^2 of the solvent-excluded area shown in Figure 2a likely account for the bulk of it. PLA2 is estimated to mask an area of 1750 Å^2 (*6*) on the interface, which would cover about 40 phospholipids, as suggested from the stoichiometry of the PLA2 binding isotherm with DTPM (*31*). These results suggest only a minor solvent accessible overhang exists. Moreover, the presence of five anion binding sites in a footprint of 40 lipids (i.e., 0.125 mole fraction) is consistent with the result that the presence of a mole fraction of 0.15 anionic amphiphile in a zwitterionic interface induces the optimum activity (*32*). According to our view of PLA2 activation, the i-face is in intimate contact with at least 30−40 phospholipid molecules, which is in stark contrast to the dual phospholipid model of Dennis in which the critical interaction for the activation requires binding of only one phospholipid (*33*).

There have been other reported examples of PLA2 structures that form a crystallographic dimer (*14*, *15*). In contrast to the S- and P-structures reported here, these structures lack an inhibitor or anions bound as part of their dimerization. In addition, the subunit contact surface in most of the crystallographic oligomers is not with the i-face that we consider critical for the interfacial binding and processive turnover. Only the Habu snake PLA2 structure (*15*) exhibits a subunit−subunit contact surface that comes close to that observed for the S- and P-structures. They reported several of the same residues in contact with the neighboring subunit, however, with several significant differences. Unfortunately, this structure is not deposited in the PDB.

Another significant aspect of the crystallographic subunit interactions is that contacts within the unit cell are inevitable. The significance of the i-face to i-face contact seen in the P- and S-structures lies in the fact that the substrate is not accessible to the active site of the dimer. To entertain the possibility of a catalytically significant allosteric dimer, one needs to invoke a structure in which the regulatory subunit interaction is not along the i-face. The possibility of a functionally active dimer form is independently discounted by evidence showing that the 14 kDa monomer is fully active at the interface (*34*).

Role of Anionic Charge in Interface Binding versus the k^*_{cat} Activation. Catalytic turnover by pancreatic PLA2 has been shown to be enhanced by anionic interface binding (*32*) and the subsequent allosteric k^*_{cat} activation (*8*). Recent studies involving site-directed mutagenesis have suggested that the binding and activation components are dependent on the charge compensation of separate cationic residues (*3*, *7*). For example, the charge compensation of Lys-120 in bovine pancreatic PLA2 influences the binding of the enzyme to the interface. In the porcine pancreatic S- and P-structures, only residue Lys-122 near the C-terminus (Figure 1a) participates directly in anion binding. On the other hand, residues Lys-53 and Lys-56, which mediate the k^*_{cat} activation of the reaction (*3*), are localized at the edge of the i-face. These residues do not directly participate in anion binding in the S- or P-structure, and therefore may not need to be embedded in the interface in the active form of the enzyme.

Features of the anion binding in Table 2 provide a rationale for the mutagenesis results where the charge compensation by Lys to Met substitution (*3*, *7*) or the charge reversal by Lys to Glu substitution (*35*−*37*) altered the K_d by less than a factor of 50. These results support the view that the direct charge compensation by cationic residues on the i-face is not necessary for binding to the anionic interface, and such a contribution may account for only 2 kcal/mol. On the other hand, the affinity of binding to a zwitterionic phosphatidylcholine interface is lowered by about 8 orders of magnitude (*32*), whereas anionic phosphatidylserine and phosphatidylglycerol interfaces show only a modest decrease of binding affinity compared to a phosphatidylmethanol interface (*31*). These results suggest that the anionic charge at the interface is critical for the binding of PLA2 with only a modest steric disruption of the i-face contacts by *sn*-3 substituents of the size of serine or glycerol. The dissection of individual contributions to binding across such a large surface offers a challenge for the future.

The Active Site Events. Features of the active site in the P- and S-structures also offer a detailed structural perspective for the environment of the tetrahedral intermediate in the chemical step. One of the more interesting interactions of hydrophobic residues from the dimer contact surface is the 69-loop. This loop is partly disordered or occupies one of two extreme positions in other reported PLA2 structures (*9*, *12*−*17*). The location of the 69-loop is potentially critical in light of its role in the chemical step (*38*) and the observed interaction of the hydroxyl of Tyr-69 with the *sn*-2 phosphate of MJ33 (Figure 1b). The Tyr-69 hydroxyl makes a notably different contact with the *sn*-3 phosphate in other substrate mimic crystal structures (*13*). Remarkably, its position differs

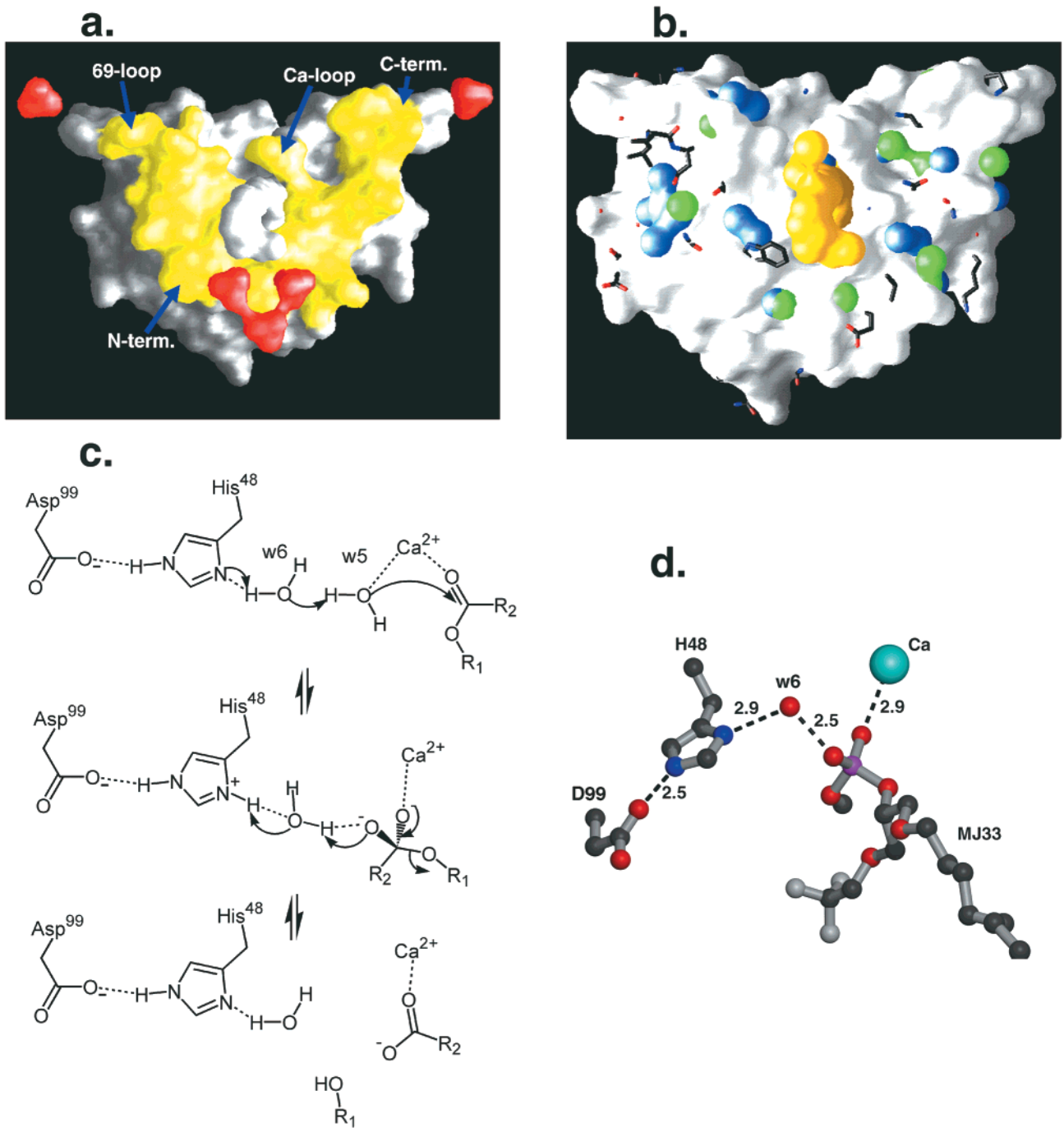

FIGURE 2: Interpreting interface binding and mechanism. (a) Footprint of PLA2 displayed using the program GRASP (*43*), which displays the van der Waals surface of the dimer contact surface of subunit A of the P-structure. The view that is shown is the subunit−subunit interface contact surface from a perspective orthogonal to the plane of bound anions. Residues that are within 5 Å of subunit B are in yellow. Bound phosphate anions are in red. In the center of the footprint is the gray alkyl tail of the MJ33 inhibitor. (b) Bound interfacial waters are in blue on the interface surface of subunit A of the P-structure. The MJ33 molecule is in yellow. The 16 interfacial waters of the P-structure all lie in a 5 Å wedge centered about the plane dissecting the subunit interface, and each water is within 4 Å of either subunit A or B. An alignment of the bovine PLA2 structure (PDB entry 1FDK) complexed with MJ33 (*12*) was performed. Waters from the bovine structure are in green, and portions of the bovine structure that project beyond the van der Waals surface of the P-structure are shown as ball-and-stick diagrams. (c) Water (w6)-assisted calcium-coordinate oxyanion (w5) mechanism of PLA2 (*38*). The assisting water is H-bonded to His-48 and remains so in the tetrahedral intermediate. The oxyanion catalytic water (w5) becomes the *pro-S* oxygen of the tetrahedral intermediate. (d) The active site of PLA2 from the P-structure has an assisting water (w6) bridging the ND1 atom of His-48 and the *pro-S* oxygen of the *sn*-2 phosphate of MJ33. Panel d was made using the programs MOLSCRIPT (*42*), POVSCRIPT (E. Peisach and D. Peisach, Brandeis University, Waltham, MA), and POVRAY (http://www.povray.org).

from that found in a structure of bovine PLA2 bound with the same inhibitor, MJ33 (*12*). This structure was determined from a protein crystal that had one subunit in the asymmetric unit and did not demonstrate the anion and i-face interactions observed in the S- and P-structures presented here.

A comparison of these structures may represent a glimpse of the key elements needed to attain the catalytically competent form. Places where the monomeric form of bovine PLA2−MJ33 (PDB entry 1FDK) differs from the P-structure are displayed in Figure 2b. The most notable difference is

shown in the 69-loop region, which reflects a restructuring that likely occurs upon interface binding. Figure 2b also reveals some differences of bound water molecules between the P-structure and the monomeric bovine structure. Interestingly, there is a notable absence of bound water molecules surrounding the alkyl tail of MJ33 that projects out of the PLA2 active site in the P-structure.

Another interesting active site feature in the P-structure is the presence of a water molecule, w6, which bridges His-48 and MJ33. This water potentially represents the assisting water (w6) between His-48 and the calcium-activated oxyanion water (w5) of the mechanism shown in Figure 2c that was originally proposed on the basis of solvent isotope effects, calcium substitution kinetics, and the ab initio docking and the coordinate search of the Eulerian space in the active site (*38*). The location of the putative assisting water w6 in relation to calcium, His-48, and Asp-49 is shown in Figure 2d from the P-structure. The *pro-S* oxygen of the *sn*-2 phosphate of MJ33 is positioned where the calcium-activated oxyanion, w5, is predicted to be located in the tetrahedral intermediate (Figure 2c). A contact of this oxygen to the hydroxyl of Tyr-69 (Figure 1b) reaffirms a role for this residue in the chemical step as seen from a 10-fold reduction in the k^*_{cat} of the Tyr-69-Phe mutant (*38*). Another functionally critical comparison to previously reported structures is that the monomeric bovine PLA2 structure complexed with MJ33 does not have this bridging water, and in fact has His-48 directly interacting with MJ33. These active site structural differences, including the position of w6, may explain the functional differences between PLA2 in its anion-activated form [$(E^*S)^{\#}$] and a less active form (E*S) (Scheme 1), which is lacking critical i-face interactions, such as bound anions. Simply put, the switch from a single-water to a water-assisted mechanism, which is supported in the P- and S-structures, may be the missing link to explain the allosteric k^*_{cat} activation (*3*) of PLA2 on an anionic interface.

Recently, a theoretical approach using quantum-mechanical/molecular-mechanical (QM/MM) calculation (*39*) has given support to the calcium-coordinate oxyanion mechanism (*38*) in which the breakdown of the tetrahedral intermediate is rate-limiting. However, the QM/MM study also predicted that a single-water mechanism is more likely to exist than the water-assisted mechanism (*39*). It should be noted that these calculations were performed starting from a monomeric crystallographic model of a venom IIB PLA2 (PDB entry 1POB). In light of our recent structural insights, it would be interesting to compare the theoretical QM/MM results starting from the interface dimer model presented in this paper to see if a water-assisted mechanism would emerge. In short, the dimeric PLA2 structures with either phosphates or sulfates bound represent a model of the enzyme in its activated state. The structural differences observed, such as the presence of an assisting water in the P- and S-structures, are likely due to anionic binding, i-face desolvation, and i-face close-contact interactions that direct this enzyme into its fully active form.

ACKNOWLEDGMENT

We thank Professors G. Sheldrick and A. Rheingold for help regarding the merohedral twinning of the S- and P-structures and Professor M. Gelb for stimulating discussions.

REFERENCES

1. Verheij, H. M., Slotboom, A. J., and de Haas, G. H. (1981) *Rev. Physiol. Biochem. Pharmacol. 91*, 91−203.
2. Jain, M. K., Gelb, M. H., Rogers, J., and Berg, O. G. (1995) *Methods Enzymol. 249*, 567−614.
3. Yu, B. Z., Poi, M. J., Ramagopal, U. A., Jain, R., Ramakumar, S., Berg, O. G., Tsai, M. D., Sekar, K., and Jain, M. K. (2000) *Biochemistry 39*, 12312−12323.
4. Jain, M. K., Rogers, J., Jahagirdar, D. V., Marecek, J. F., and Ramirez, F. (1986) *Biochim. Biophys. Acta 860*, 435−447.
5. Berg, O. G., Yu, B. Z., Rogers, J., and Jain, M. K. (1991) *Biochemistry 30*, 7283−7297.
6. Ramirez, F., and Jain, M. K. (1991) *Proteins 9*, 229−239.
7. Rogers, J., Yu, B. Z., Tsai, M. D., Berg, O. G., and Jain, M. K. (1998) *Biochemistry 37*, 9549−9556.
8. Berg, O. G., Rogers, J., Yu, B. Z., Yao, J., Romsted, L. S., and Jain, M. K. (1997) *Biochemistry 36*, 14512−14530.
9. Yuan, C., and Tsai, M. (1999) *Biochim. Biophys. Acta 1441*, 215−222.
10. Ball, A., Nielsen, R., Gelb, M. H., and Robinson, B. H. (1999) *Proc. Natl. Acad. Sci. U.S.A. 96*, 6637−6642.
11. Lin, Y., Nielsen, R., Murray, D., Hubbell, W. L., Mailer, C., Robinson, B. H., and Gelb, M. H. (1998) *Science 279*, 1925−1929.
12. Sekar, K., Eswaramoorthy, S., Jain, M. K., and Sundaralingam, M. (1997) *Biochemistry 36*, 14186−14191.
13. Scott, D. L., and Sigler, P. B. (1994) *Adv. Protein Chem. 45*, 53−88.
14. Brunie, S., Bolin, J., Gewirth, D., and Sigler, P. B. (1985) *J. Biol. Chem. 260*, 9742−9749.
15. Suzuki, A., Matsueda, E., Yamane, T., Ashida, T., Kihara, H., and Ohno, M. (1995) *J. Biochem. 117*, 730−740.
16. Finzel, B. C., Ohlendorf, D. H., Weber, P. C., and Salemme, F. R. (1991) *Acta Crystallogr. B47*, 558−559.
17. Dijkstra, B. W., Kalk, K. H., Hol, W. G., and Drenth, J. (1981) *J. Mol. Biol. 147*, 97−123.
18. Jain, M. K., Tao, W. J., Rogers, J., Arenson, C., Eibl, H., and Yu, B. Z. (1991) *Biochemistry 30*, 10256−10268.
19. Otwinowski, Z., and Minor, W. (1997) *Methods Enzymol. 276*, 307−326.
20. Collaborative Computational Project No. 4 (1994) *Acta Crystallogr. D50*, 760−763.
21. Brunger, A. T. (1992) *X-PLOR Version 3.1. A system for X-ray Crystallography and NMR*, Yale University Press, New Haven, CT.
22. Sack, J. S., and Quiocho, F. A. (1997) *Methods Enzymol. 277*, 158−173.
23. Jones, T. A., Zou, J. Y., Cowan, S. W., and Kjeldgaard, M. (1991) *Acta Crystallogr. A47*, 110−119.
24. Yeates, T. O. (1997) *Methods Enzymol. 276*, 344−358.
25. Redinbo, M. R., Cascio, D., Choukair, M. K., Rice, D., Merchant, S., and Yeates, T. O. (1993) *Biochemistry 32*, 10560−10567.
26. Brunger, A. T., Adams, P. D., Clore, G. M., Delano, W. L., Gros, P., Grosse-Kunstleve, R. W., Jiang, J.-S., Kuszewski, J., Nilges, N., Pannu, N. S., Read, R. J., Rice, L. M., Simonson, T., and Warren, G. L. (1998) *Acta Crystallogr. D54*, 905−921.
27. Sheldrick, G. M. (1998) in *Direct Methods for Solving Macromolecular Structures* (Fortier, S., Ed.) pp 401−411, Kluwer Academic Publishers, Dordrecht, The Netherlands.
28. Chakrabarti, P. (1993) *J. Mol. Biol. 234*, 463−482.
29. Deisenhofer, J., Epp, O., Sinning, I., and Michel, H. (1995) *J. Mol. Biol. 246*, 429−457.

30. Jain, M. K., DeHaas, G. H., Marecek, J. F., and Ramirez, F. (1986) *Biochim. Biophys. Acta 860*, 475−483.
31. Jain, M. K., Rogers, J., Marecek, J. F., Ramirez, F., and Eibl, H. (1986) *Biochim. Biophys. Acta 860*, 462−474.
32. Jain, M. K., Egmond, M. R., Verheij, H. M., Apitz-Castro, R., Dijkman, R., and De Haas, G. H. (1982) *Biochim. Biophys. Acta 688*, 341−348.
33. Lefkowitz, L. J., Deems, R. A., and Dennis, E. A. (1999) *Biochemistry 38*, 14174−14184.
34. Jain, M. K., Ranadive, G., Yu, B. Z., and Verheij, H. M. (1991) *Biochemistry 30*, 7330−7340.
35. Koduri, R. S., Baker, S. F., Snitko, Y., Han, S. K., Cho, W., Wilton, D. C., and Gelb, M. H. (1998) *J. Biol. Chem. 273*, 32142−32153.
36. Ghomashchi, F., Lin, Y., Hixon, M. S., Yu, B. Z., Annand, R., Jain, M. K., and Gelb, M. H. (1998) *Biochemistry 37*, 6697−6710.
37. Lin, Y., Ghomashchi, F., Nielsen, R., Snitko, Y., Yu, B. Z., Han, S. K., Cho, W., Wilton, D. C., Jain, M. K., Robinson, B. H., and Gelb, M. H. (1998) *Biochem. Soc. Trans. 26*, 341−345.
38. Yu, B. Z., Rogers, J., Nicol, G. R., Theopold, K. H., Seshadri, K., Vishweshwara, S., and Jain, M. K. (1998) *Biochemistry 37*, 12576−12587.
39. Schurer, G., Lanig, H., and Clark, T. (2000) *J. Phys. Chem. B 104*, 1349−1361.
40. Brunger, A. T. (1992) *Nature 355*, 472−474.
41. Lee, B., and Richards, F. M. (1971) *J. Mol. Biol. 55*, 379−400.
42. Kraulis, P. J. (1991) *J. Appl. Crystallogr. 24*, 946−950.
43. Honig, B., and Nicholls, A. (1995) *Science 268*, 1144−1149.

BI002514G